

Propagation dynamics of optical vortices

D. Rozas

Department of Physics, Worcester Polytechnic Institute, Worcester, Massachusetts 01609-2280

C. T. Law

Department of Electrical Engineering and Computer Science, University of Wisconsin, Milwaukee, Wisconsin 53201

G. A. Swartzlander, Jr.

Department of Physics, Worcester Polytechnic Institute, Worcester, Massachusetts 01609-2280

Received January 21, 1997; revised manuscript received March 28, 1997

Optical vortices in linear and nonlinear media may exhibit propagation dynamics similar to hydrodynamic vortex phenomena. Analytical and numerical methods are used to describe and investigate the interaction between vortices and the background field. We demonstrate that optical vortices that have quasi-point core functions, such as optical vortex solitons, may orbit one another at rates that are orders of magnitude larger than those with nonlocalized cores. © 1997 Optical Society of America [S0740-3224(97)01811-0]

1. INTRODUCTION

From early experiments in optics and acoustics it was found that field vortices are generated when waves scatter from rough surfaces.¹⁻⁴ An optical vortex (OV) also occurs as a particular solution to the wave equation in cylindrical coordinates; hence the doughnut mode of a laser cavity is an example of an OV.⁵⁻¹⁷ For this reason, large-area lasers and other resonators have been examined for the spontaneous birth and dynamics of OV modes.¹⁸⁻²⁵ The advent of computer-generated holography later opened new opportunities to investigate arbitrary configurations involving optical vortices (OV's)^{26,27} permitting, for example, the observation of fluidlike rotations of quasi-point OV's.²⁸ Simultaneously, other intriguing questions were being explored.²⁹⁻³⁵ During this time, vortices in nonlinear optics were also being discussed, and in 1992 the optical vortex soliton (OVS) was observed.^{36,37} Not only was the soliton observed for a beam containing some initial vorticity, but pairs of vortices with opposite topological charges were experimentally observed to develop spontaneously, owing to a Kelvin-Helmholtz-type snake instability.^{36,38-41} Preliminary analyses of the OVS⁴²⁻⁴⁴ were followed by other theoretical investigations: vortex birth by means of nonlinear instability,⁴⁵⁻⁴⁷ stable^{48,49} and unstable⁴⁸ polarization effects, higher-order nonlinearities,⁵⁰ propagation dynamics,^{41,51} and other effects.⁵² Exotic OV-atom interactions involving anyonic statistics have also been proposed.⁵³ Most recently, nonlinear refractive phenomena have been investigated in photorefractive media^{38-40,54,55} that are biased into the Kerr-like regime⁵⁶ and in atomic vapors.^{41,51,57,58} Vortices are known to profoundly affect the physical properties of systems such as superfluids and superconductors;⁵⁹⁻⁶² thus research into OV phenomena may also provide surprising and potentially useful new optical

phenomena. Already the radiation pressure and angular momentum from OV's have been used to manipulate small particles and atoms.⁶³⁻⁶⁸

OVS's are intriguing not only because they are the only known $(2 + 1)$ -dimensional solitons in Kerr-like media but also because they may exhibit propagation dynamics distinctly different from those of vortices that occur as cavity modes. As described here, this difference is attributed in large part to the amplitude profile of the vortex core. This difference can also be observed in linear media when one examines the propagation of vortices that have small localized core functions rather than the wide global core functions that characterize cavity modes. For cavity-type modes the amplitude of the electric field varies linearly with the radial distance from the vortex core, and thus we shall call it an r vortex. In the case of OVS's or other localized cores, the amplitude can be modeled as $\tanh(r/w_v)$, and we shall call this a \tanh vortex. As the size of the \tanh vortex vanishes ($w_v \rightarrow 0$) the vortex is said to become a point vortex.

This paper was written to help develop an intuitive understanding of OV motion and to describe the propagation characteristics of different types of vortices in linear and nonlinear media. For example, in a linear material a single vortex of any type moves across a Gaussian beam in a straight line when the vortex is placed off center (it does not rotate, as is sometimes described). We also give detailed accounts of the orbital motion of identical quasi-point vortices in linear and nonlinear media and demonstrate how the rotation can slow and reverse its direction. In Section 2 we review the definitions and properties of OV's. Analytical descriptions of the propagation dynamics are presented in Section 3, followed in Section 4 by numerical and revised theoretical analyses for special cases and in Section 5 by conclusions.

2. DESCRIPTION OF OPTICAL VORTICES

In general, the vector wave equation admits cylindrical wave solutions that are characterized by a separable phase term, $\exp(im\theta)$, where θ is the azimuthal coordinate in the transverse plane and m is a signed integer called the topological charge. Here we shall consider only the case of $|m| = 1$ (we can account for higher charges by treating multiple singly charged vortices). We shall refer to this phase term as the vortex term, owing to the special properties, such as particlelike propagation (even in linear media), conservation of charge, and conservation of angular momentum, that it exhibits in an optical system. We shall make the paraxial wave approximation, with the waves propagating along the $+z$ direction and oscillating as $\exp[i(\omega t - kz)]$, where ω is the frequency, $k = 2\pi/\lambda$ is the wave number, and λ is the wavelength. To simplify the description of the propagation dynamics owing to diffraction, the scalar wave equation is used. The propagation of vortices through nonlinear refractive media can also be described by a scalar equation, assuming either that the material exhibits no nonlinear polarizability or that the light is circularly polarized.^{48–49} Using cylindrical coordinates, we can express the field of a single vortex with the ansatz

$$\begin{aligned} E(r, \theta, z) &= E_0 G_{\text{bg}}(r, z) \exp[i\Phi(r, z)] \\ &\quad \times A(r, z) \exp(im\theta) \exp(-ikz) \\ &= E_0 u(r, \theta, z) \exp(-ikz), \end{aligned} \quad (1)$$

where E_0 is a characteristic amplitude; $\Phi(r, z)$ describes the part of the phase that changes as the beam propagates; $A(r, z)$ describes the amplitude profile of the vortex core; G_{bg} describes the amplitude of the background field in which the vortex exists; and u is a normalized slowly varying complex function. We have dropped the factor $\exp(i\omega t)$; in the laboratory reference frame the dynamics occurs as the beam propagates through space, not time. Unless stated otherwise, we shall assume that the background field has a Gaussian profile: $G_{\text{bg}}(r, z) = \exp[-r^2/w^2(z)]$, where $w(z)$ characterizes the beam size. We shall compare and contrast two characteristically different vortex core functions: a tanh vortex (used, for example, to describe OVS's),

$$A(r, z = 0) = \tanh(r/w_v), \quad (2)$$

and an r vortex (found, for example, in a beam emerging from a cylindrical waveguide),

$$A(r, z = 0) = (r/w_r)^{|m|}, \quad (3)$$

where the vortex core size is characterized by w_v in Eq. (2) but not by w_r in Eq. (3). In the latter case, the measurable core size is not an independent parameter but rather is characterized by the background beam; for a Gaussian background, the half-width at half-intensity maximum of the core is $w_{\text{HWHM}} \approx 0.59w_0$. The parameter w_r is an arbitrary length that, together with E_0 , simply scales the peak intensity of the beam. The intensity profiles for the fields, Eqs. (2) and (3), contain a noticeable dark vortex core whose intensity is zero at the center, as shown for an r vortex and a tanh vortex in Fig. 1.

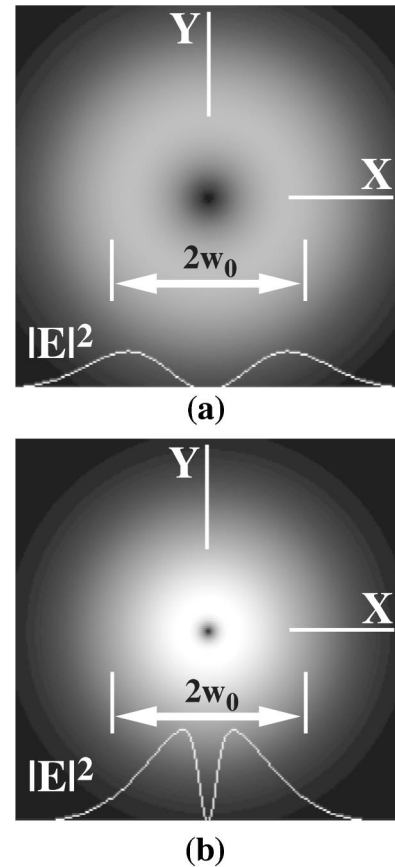


Fig. 1. Intensity profiles of (a) an r vortex and (b) a tanh vortex upon a Gaussian background beam of size w_0 , showing the respective large and small vortex core sizes. The images are shown with a logarithmic gray-scale pallet, whereas a linear scale is used for the line plots (this applies to the other figures, unless noted).

First let us review the equations that describe vortex (or doughnut) modes that may emerge from a cylindrically symmetric laser cavity. These modes belong to a family of solutions described by Eq. (1), where $A(r, z)$ are Laguerre polynomials.⁵ We are interested now only in those solutions that exhibit at most one intensity minimum within the beam. In that case the solution at the beam waist ($z = 0$) is given by Eq. (3), where $w_r = 2^{-1/2}w_0$. It is well known that the propagation of an r vortex in a Gaussian beam is similar to that of an $m = 0$ beam (the TEM_{00} mode).⁶⁹ The amplitude is a self-similar function described by $[w_0/w(z)] \times [r/w(z)]^{|m|} \exp[-r^2/w^2(z)]$, where $w(z) = w_0[1 + (z/Z_0)^2]^{1/2}$ and $Z_0 = \pi w_0^2/\lambda$ are the beam size and the characteristic diffraction length, respectively. In this case the changing phase term in Eq. (1) is given by $\Phi(r, z) = (m + 1)\Phi_G(z) + kr^2/2R(z)$, where

$$\Phi_G(z) = \arctan(z/Z_0) \quad (4)$$

is the “dynamic” Gouy shift, and $R(z) = z[1 + (Z_0/z)^2]$ is the radius of curvature of the wave front. The Gouy shift⁷⁰ accounts for the 180° inversion of a beam as it propagates from $z = -\infty$ to $z = +\infty$ with a focal region (the waist) at $z = 0$ (or a 90° rotation from $z = 0$ to $z = \infty$).

Next we describe the field of an OVS, which has been observed in self-defocusing nonlinear refractive media.^{36,54} A closed-form expression for the field does not exist, but a convenient model equation^{59–61} for the vortex core function is given by Eq. (2). In practice a beam with this core function can be formed by use of computer-generated holograms^{26,27} or of a diffractive optical element that has an etched surface resembling a spiral staircase,^{15,16} although it will not propagate unchanged in linear media. Figure 1 shows the intensity profiles of two beams that have the same-sized background beam and power for an r vortex and a tanh vortex. The tanh vortex core size may be arbitrarily small, and hence the peak intensity may be as much as $e = 2.71$ times greater than that of an r vortex beam, provided that the total power and the Gaussian beam size are the same.

The propagating field of a point vortex ($w_v = 0$) can also be determined analytically by integration of the paraxial Fresnel integral.⁷¹ We find that

$$G_{\text{bg}}(r, z)A_m(r, z) = \frac{\pi^{1/2}}{2} \frac{r}{w_0} \left(\frac{Z_0}{z}\right)^{1/2} \left[\frac{Z_0}{R(z)}\right]^{3/2} \times [I_{\nu(-)}(\gamma) - I_{\nu(+)}(\gamma)] \exp\left[-\frac{1}{2} \frac{r^2}{w^2(z)}\right], \quad (5)$$

$$\Phi(r, z) = (\pi/2)(3/2 - m) + (Z_0/z)(r/w_0)^2 \times [1 - (1/2)w_0^2/w^2(z)] - (3/2)\arctan(z/Z_0), \quad (6)$$

where $I_\nu(\gamma)$ is the modified Bessel function of the first kind of fractional order $\nu^{(\pm)} = (m \pm 1)/2$, $w(z)$ is described above, and the argument $\gamma = (1/2)[r/w(z)]^2(1 + iZ_0/z)$. The intensity profile, $|A_m|^2$, is characterized by high spatial frequency ringing in the near field, $z/Z_0 \ll 1$, and smooth profiles for $z/Z_0 > 1$. The intensity profiles are described and depicted in Section 4 below. As the beam propagates to infinity, $\gamma \rightarrow 0$ and the difference of the modified Bessel functions tends to unity.

3. VORTEX PROPAGATION DYNAMICS

Ginzburg and Pitaevskii⁵⁹ and Pitaevskii⁶⁰ reported stationary vortex solutions to an equation that was later called the nonlinear Schrödinger equation. In the context of diffractive optics, this equation is written as

$$-2ik(\partial u/\partial z) + \nabla_\perp^2 u + 2k^2(n_2 E_0^2/n_0)|u|^2 u = 0, \quad (7)$$

where $\nabla_\perp^2 u = (1/r)[\partial/\partial r(r\partial u/\partial r)] + (1/r^2)(\partial^2 u/\partial \theta^2)$ is the transverse Laplacian in cylindrical coordinates, u is the envelope defined in Eq. (1), n_2 is the coefficient of nonlinear refractive index ($n_2 < 0$ for self-defocusing media), and n_0 is the linear index of refraction. That earlier research had a significant effect on the fields of superfluidity and superconductivity. An understanding of OV phenomena can now benefit from the progress made in those areas because the nonlinear Schrödinger equation describes the propagation of scalar paraxial waves in both linear and nonlinear media, which correspond to the nor-

mal and the condensate states, respectively. In optics the normal state may remain coherent, whereas the coherence is typically lost to phonons and other perturbations when the Bose condensate experiences a phase transformation to the normal state.

Hydrodynamic paradigms have been used to describe electromagnetic phenomena throughout history. The nonlinear Schrödinger equation follows this tradition, as it has been shown to transform into two of the principal equations in fluid mechanics: the Bernoulli and the continuity equations.^{72,73} One can obtain these equations by writing the complex field envelope $u = f(r, \theta, z)\exp[is(r, \theta, z)]$. Inserting this expression into Eq. (7), one obtains two coupled equations:

$$-\partial s/\partial z + \mathbf{k}_\perp \cdot \mathbf{k}_\perp = \nabla_\perp^2 \rho^{1/2}/\rho^{1/2} - P/\rho, \quad (8)$$

$$(1/2)\partial \rho/\partial z + \nabla_\perp \cdot (\rho \mathbf{k}_\perp) = 0, \quad (9)$$

where $\mathbf{k}_\perp = -\nabla_\perp s$ is the transverse wave vector, or momentum (in units of \hbar), of the beam (it is analogous to the velocity field of a fluid) and $\rho = f^2$ (the intensity) and $P = 2\rho^2$ are analogous to the density and the pressure of a fluid, respectively. The term P/ρ in Eq. (8) vanishes in linear media ($n_2 = 0$). From Eq. (1) we write $s = m\theta + \Phi(r, z)$ and $f = G_{\text{bg}}(r, z)A(r, z)$. It is clear from Eqs. (8) and (9) that two of the important terms driving the propagation dynamics in both linear and nonlinear media are the phase gradient \mathbf{k}_\perp and the intensity gradient $\nabla_\perp \rho$.

At all points, except the singularity, we find that

$$\mathbf{k}_\perp = -\nabla_\perp s = -\hat{\theta}r^{-1}\partial s/\partial \theta - \hat{r}\partial s/\partial r. \quad (10)$$

Special attention is needed to describe the field dynamics at the singularity. In a fluid, one finds that the velocity field at the center of the vortex is unaffected by the vortex itself; rather, the vortex can be viewed as being attached to a particle that moves with the local flow field. In a similar fashion, the transverse wave vector at the center of an OV is unaffected by the vortex itself. The trajectory of a given vortex is affected by all other sources of \mathbf{k}_\perp and $\nabla_\perp \rho$, such as diffracting waves and other vortices. The fluid paradigm suggests the following hypothesis for an OV: In a linear medium the vortex trajectory is affected by the factors in the field at the singularity that exclude the singularity being examined, i.e., the field $u/[A(r, z)\exp(im\theta)]$ and its derivatives, evaluated at the vortex core. Thus at the center of the vortex core the transverse momentum is $\mathbf{k}_\perp = -\nabla_\perp \Phi$ (this may also be viewed as the local average value of \mathbf{k}_\perp in the vicinity of the core). To develop an understanding of the effects of amplitude and phase gradients on vortex motion, let us consider these two interactions separately.

To demonstrate that a vortex moves perpendicularly to the gradient of the background field in a linear medium, let us consider a vortex of charge ($m = \pm 1$) in the presence of a background field having a constant gradient:

$$E(r, \theta, z = 0) = E_0 \exp(im\theta)[1 + (r/L)\cos\theta]/w_r, \quad (11)$$

where L and w_r characterize the slope of the background field and the vortex core, respectively. {Note that $|L^{-1}| = |G_{\text{bg}}^{-1}\nabla_\perp G_{\text{bg}}|_{r=0}$, where $G_{\text{bg}} = E_0[1 + (r/L)\cos\theta]$ }

As the beam propagates, one can easily determine the initial direction of motion of the vortex by expressing the field (or the intensity) as a Taylor-series expansion: $u(r, \theta, \delta z) = u(r, \theta, 0) + (\partial u / \partial z) \delta z$, where $\partial u / \partial z$ can be found from Eq. (7) [a similar exercise can be conducted with Eq. (9)]. The coordinates of the vortex must satisfy the condition $|u| = 0$, whence we find the vortex displacement vector:

$$\mathbf{r}(\delta z) = \text{sgn}(m)(\delta z/k^2)\mathbf{k} \times (G_{\text{bg}}^{-1}\nabla_{\perp}G_{\text{bg}})_{r=0}, \quad (12)$$

where $\text{sgn}(m) = m/|m|$. Thus the vortex moves not in the direction of the sloping field but rather perpendicular to it. If the topological charge is positive (negative), the vortex moves in the positive (negative) y direction. This demonstration suggests that a vortex that has an arbitrary core function can experience a displacement whenever the intensity of the background field is nonuniform.

Let us now examine the motion of a vortex in the presence of a nonuniform phase. In particular, we shall consider the fundamental interaction between two identical vortices separated by a distance d , shown schematically in Fig. 2. To obtain a purely phase-dependent interaction, with no amplitude-dependent effects as previously described, we assume point vortices ($w_v \rightarrow 0$) on an infinite, uniform-background field ($w_0 \rightarrow \infty$). We note that the vortex cores will diffract over some distance of order $Z_V = \pi d^2/\lambda$, and thus the background field experienced by each vortex will appear nonuniform for $|z| \gtrsim Z_V$. However, over the range $|z| \ll Z_V$, the background field can be considered uniform and is approximated by

$$E(r, \theta, z) = \exp[i(m_1\theta_1 + m_2\theta_2) - ikz], \quad (13)$$

where θ_j is the azimuthal coordinate measured about the j th vortex, which has a topological charge, m_j (Fig. 3). We wish to find the angular displacement ϕ of a propagating vortex from its initial position, $\Theta_j(z=0)$:

$$\phi(z) \equiv \Theta_j(z) - \Theta_j(z=0). \quad (14)$$

For simplicity, let us assume that $m_1 = m_2 = -1$. In this case the transverse wave vector at all nonsingular points is determined from Eq. (10):

$$\mathbf{k}_{\perp} = \hat{\theta}_1/r_1 + \hat{\theta}_2/r_2, \quad (15)$$

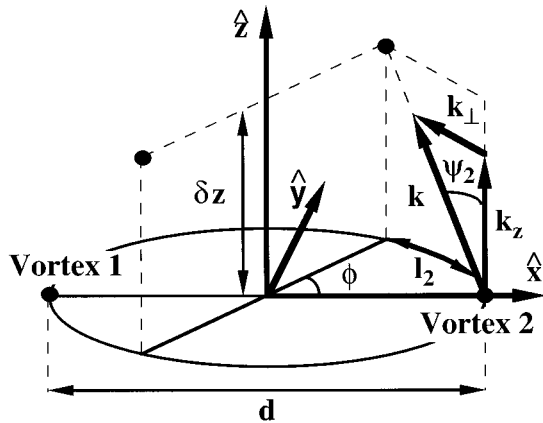


Fig. 2. Three-dimensional sketch of the position of the vortex in the transverse x - y plane, propagating in the z direction with wave vector $\mathbf{k} \approx k_z \hat{z}$. The wave vector at the center of vortex 2 has a transverse component $\mathbf{k}_{\perp} \approx \mathbf{k}_2$.

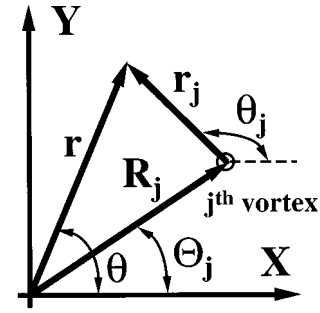


Fig. 3. Transverse coordinates of the j th vortex, located at point (R_j, Θ_j) with respect to the origin (assumed to be at the center of the background beam). The amplitude and the phase of the vortex are expressed in terms of coordinates (r_j, θ_j) .

where $\hat{\theta}_j$ is the unit vector along the azimuth of the j th vortex and r_j is the distance from its center. However, at the center of vortex 1 the effective wave vector is $\mathbf{k}_{\perp}(r_1 = 0) = \hat{\theta}_2/d$. Likewise, at the center of vortex 2, $\mathbf{k}_{\perp}(r_2 = 0) = \hat{\theta}_1/d$. The transverse wave vector at the singularities indicates the direction of motion of the vortices in the transverse plane. Combining the transverse and longitudinal motions, one may expect the two vortices to trace a double-helical trajectory, analogous to the orbital motion in time of two vortices in a fluid.⁷⁴ This trajectory can be determined with the aid of Fig. 2. The angle ψ_2 between the transverse wave vector at vortex 2 and the optical axis \hat{z} can be determined from trigonometry:

$$\tan \psi_2 = k_{\perp}(r_2 = 0)/k = \lambda/(2\pi d), \quad (16)$$

where the paraxial wave approximation, $k_{\perp} \ll k_z \approx k$, has been assumed. While propagating a distance z in the \hat{z} direction, vortex 2 moves an arc length, $l_2 = z \tan \psi_2$, in the transverse plane around the point at the center of the pair (the origin), which is located a distance $d/2$ from each vortex. The angle of rotation is then

$$\phi = 2l_2/d = (2/d)z \tan \psi_2. \quad (17)$$

We can now find the angular rate of rotation, using Eqs. (16) and (17):

$$\Omega_d \equiv d\phi/dz = \lambda/(\pi d^2) = 1/Z_V. \quad (18)$$

An equivalent result was obtained by Roux, who used another approach.¹⁷ Our numerical calculations, described below, indicate that Eq. (18) is valid until the vortex core functions overlap, which occurs at a distance of roughly $Z_V/4$. Thereafter, the vortex motion is found to be characteristically different (usually the angular velocity decreases), owing to the additional effects of amplitude gradients. Corrections to Eq. (18) for \tanh , rather than \tan , point, vortices are described in Section 4.

Having these examples of amplitude- and phase-driven vortex motion as conceptual guides, we now explore the more realistic case of vortex motion within a finite-sized Gaussian beam. In particular, we are interested in the trajectory of a pair of identical singly charged vortices placed symmetrically about the center of the beam in the initial plane $z = 0$. The field in this case can be written as

$$E(r, \theta, 0) = E_0 \exp(-r^2/w_0^2) \exp(-ikz) \prod_{j=1}^M A_j(r_j, 0) \times \exp(im_j \theta_j), \quad (19)$$

where $A_j(r_j, z=0)$ is the initial core function of the j th vortex, M is the number of singly charged vortices, and (r_j, θ_j) are the polar coordinates measured with respect to the center of the j th vortex (Fig. 3). We shall assume that $M=2$ and $m_1 = m_2 = -1$. The intensity profiles for tanh vortex and r vortex core functions are shown, respectively, in Figs. 4 and 5. In both cases the vortices are separated by a distance d , and the initial phase profiles (at $z=0$) shown in Fig. 6 are identical. Note that the phase increases from 0 to 2π in a clockwise sense for both vortices. The unavoidable overlap of the r vortex cores is clearly evident in Fig. 5.

The motion of r vortices in a single beam has been treated by Indebetouw,¹⁴ and we shall review his results, which, surprisingly, indicate that r vortices (unlike point vortices) exhibit no fluidlike motion. In fact, Indebetouw showed that any number of identical r vortices within a Gaussian beam will propagate independently of the others. For a single pair, as described in Eq. (19) with $A_j = r_j/w_r$, the trajectory is given, in cylindrical coordinates measured about the center of the beam (see Fig. 3), by the expressions

$$R_j(z) = R_j(0)(1 + z^2/Z_0^2)^{1/2}, \quad (20)$$

$$\Theta_j(z) = \Theta_j(0) - \text{sgn}(m)\Phi_G(z), \quad (21)$$

where $R_j(0)$ and $\Theta_j(0)$ are the initial coordinates of the j th vortex. We find that the vortices do not actually rotate, as one may expect from Eq. (21); rather the projections of the trajectories onto the transverse plane are straight parallel lines given by parametric equations:

$$y_j(z) = x_j(z) \tan[\Theta_j(0) - \text{sgn}(m)\Phi_G(z)], \quad (22)$$

where $R_j^2(0) = x_j^2(0) + y_j^2(0)$ is the initial displacement of the j th vortex from the center of the beam. Although the vortices do not circle the optical axis, it is useful to calculate the angular rate of rotation for an r vortex, using Eqs. (21) and (14):

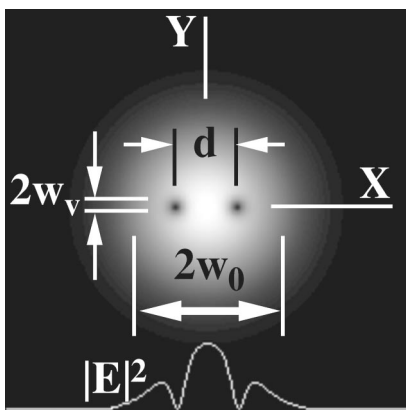


Fig. 4. Two tanh vortices of size w_v and separation d placed symmetrically about the center of a Gaussian background beam of size w_0 .

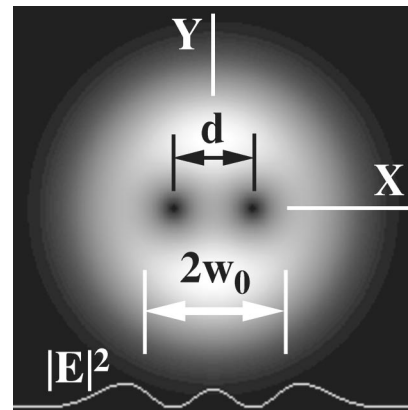


Fig. 5. Two r vortices of separation d placed symmetrically about the center of a Gaussian background beam of size w_0 .

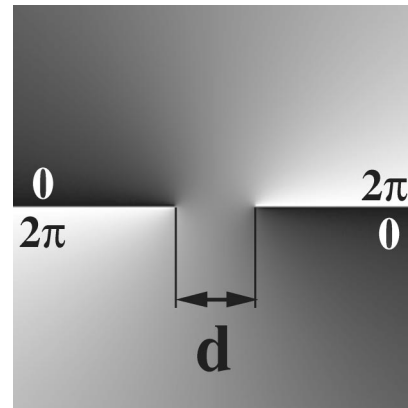


Fig. 6. Phase profile of two vortices of charge $m = -1$ in the initial transverse plane, $z = 0$, separated by a distance d . A linear gray-scale pallet was used in this case, where black (white) corresponds to a phase of 0 (2π).

$$\begin{aligned} \Omega_r &= d\phi/dz = -\text{sgn}(m)Z_0^{-1}[w_0/w(z)]^2 \\ &= -\text{sgn}(m)Z_0^{-1}[1 + (z/Z_0)^2]^{-1}. \end{aligned} \quad (23)$$

Comparing the interaction between pointlike and r vortices, we find that, whereas quasi-point vortices exhibit distance-dependent rotation rates, those with overlapping core functions tend to be independent of the vortex separation distance. To examine the motion of vortices in a Gaussian beam, numerical techniques are helpful, especially when we consider nonlinear propagation.

4. NUMERICAL INVESTIGATION

Numerical investigations not only may provide considerable insight into the physics of optical vortex propagation dynamics but also may help identify physically realizable experiments. In this section we examine four different vortex propagation phenomena that occur within a Gaussian background field. Case 1 examines the linear propagation of a single r or tanh vortex in the center of a Gaussian beam. Case 2 explores the vortex-beam interaction that occurs when a vortex is displaced from the optical axis. Vortex-vortex interactions in a linear medium are investigated in case 3 and show distinct

differences between the r and the tanh vortices. Case 4 examines the interaction between OVS's in nonlinear media.

We used the so-called split-step or beam-propagation numerical method⁷⁵ to determine the field of the propagating beam. The data were computed on a DEC-Alpha 3000-800 computer, and a Macintosh II-fx computer was used to process the images. The transverse numerical grid size was 1024×1024 (or 2048×2048 for some cases), with each element having a size $\Delta x = 4.88 \mu\text{m}$. Unless stated otherwise, a beam size of $w_0 = 488 \mu\text{m}$ and a wavelength of $\lambda = 800 \text{ nm}$ were used. For the tanh vortex cases we assume that $w_v = 57 \mu\text{m}$, which corresponds to a soliton with an induced index change of $\Delta n = 1.6 \times 10^{-5}$. Gray-scale intensity profiles are shown with a logarithmic palette to depict a visual image, whereas linear scales are used for line plots and phase profiles.

A. Case 1

The linear propagation of a vortex placed in the center of a Gaussian beam [see Eq. (1)] was described in Section 2 for an r and a point vortex. The self-similar intensity profile of a propagating r vortex is shown in Fig. 1(a). The solution for a propagating tanh vortex is intractable unless the core size vanishes [see Eqs. (5) and (6)], and thus numerical solutions are required. The discussion of Eq. (5) suggests that diffractive ringing may occur in the near-field region, even when $w_v \neq 0$. This ringing is depicted in Fig. 7 for $w_v/w_0 = 0.12$ and $w_v/w_0 = 0$, showing that intensity ringing is negligible unless $w_v/w_0 \ll 1$ (these profiles were computed at a propagation distance $z = 0.05Z_0$). For any ratio $w_v/w_0 \ll 1$, the rings diffract out of the vortex region for $z > Z_0$, and the optical quality of the beam remains smooth.

B. Case 2

Let us now displace the vortex from the center of the beam to a point where the background intensity gradient is nonzero and examine the position of the propagating vortex. As discussed in Section 3, the projection of the vortex trajectory in the transverse plane is expected to move initially in the direction of $m\mathbf{k} \times \nabla_{\perp} G_{\text{bg}}$. Let us first consider an r vortex of charge $m = +1$ placed at the point $(x_0, y_0) = (r_0, 0)$ or, equivalently, at $[R(0), \Theta(0)] = (r_0, 0)$, where $r_0 = 244 \mu\text{m}$. The initial field is given by Eqs. (3) and (19), with $M = 1$, $\theta_1 = \arctan[(y - y_0)/(x - x_0)]$, and $r_1 = [(x - x_0)^2 + (y - y_0)^2]^{1/2}$. As expected from Eq. (22), we can see from Fig. 8 that the vortex indeed moves in a straight line, with the angular position moving clockwise with respect to the center of the Gaussian beam.

We suggested in Section 3 a hypothesis that vortex motion is unaffected by its own amplitude and phase. Thus a single tanh vortex on a Gaussian beam is expected also to move in a straight line. [The field of an off-center tanh vortex can be written as in the previous example, except with the core function given by Eq. (2).] The numerically computed position of the tanh vortex, shown in Fig. 9, is indeed identical to that of the r vortex in Fig. 8. Only the

diffraction of the vortex core distinguishes these two examples. This result supports the validity of the OV hypothesis in a linear medium.

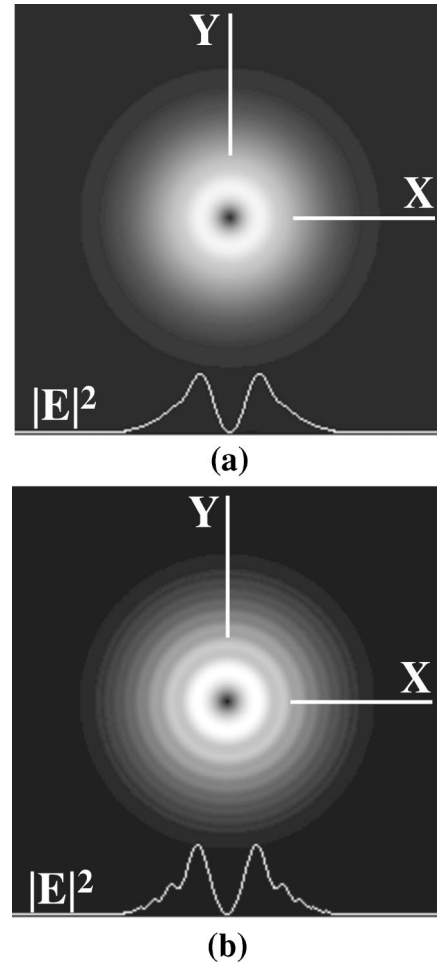


Fig. 7. Near-field intensity profiles at a propagation distance $z/Z_0 = 0.05$ showing (a) negligible ringing when $w_v = 57 \mu\text{m}$ and (b) significant vortex radiation when $w_v = 0$. The size of the initial background Gaussian field is $w_0 = 488 \mu\text{m}$.

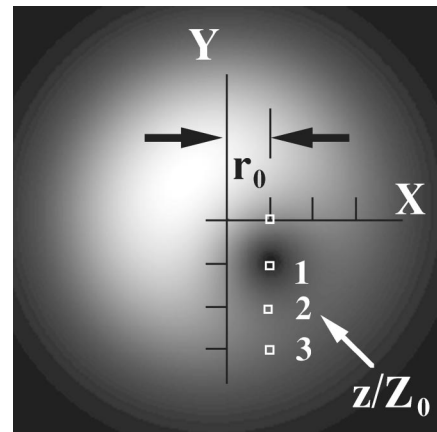


Fig. 8. Off-center r vortex of charge $m = +1$ in a Gaussian beam ($w_0 = 488 \mu\text{m}$) initially placed at point $(x_0, y_0) = (r_0, 0)$, where $r_0 = 244 \mu\text{m}$. The beam is shown at a distance $z = Z_0$. The projection of the vortex trajectory in the transverse plane, shown by the white open squares, is a straight line. The vortex advances at a uniform rate given by r_0/Z_0 .

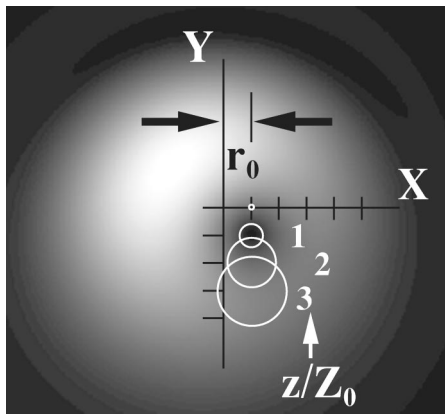


Fig. 9. Off-center tanh vortex of charge $m = +1$ in a Gaussian beam ($w_0 = 488 \mu\text{m}$) initially placed at point $(x_0, y_0) = (r_0, 0)$, where $r_0 = 244 \mu\text{m}$. The beam is shown at a distance $z = Z_0$. The projection of the vortex trajectory in the transverse plane, shown by the white open circles (whose radii depict the size of the advancing vortex), is a straight line. As for an r vortex, the tanh vortex advances at a uniform rate given by r_0/Z_0 .

C. Case 3

Let us now introduce a second vortex into the beam so that the trajectory of a vortex is affected not only by the Gaussian background field but also by the field of the other vortex. We examine the case in which the vortices, separated by a distance d and having a topological charge $m_1 = m_2 = +1$, are placed symmetrically about the center of the beam, as shown in Fig. 4 for tanh vortices and in Fig. 5 for r vortices.

The field is described by Eq. (19) with $M = 2$, $r_1 = [(x - x_{1,0})^2 + (y - y_{1,0})^2]^{1/2}$, $r_2 = [(x - x_{2,0})^2 + (y - y_{2,0})^2]^{1/2}$, $\theta_1 = \arctan[(y - y_{1,0})/(x - x_{1,0})]$, and $\theta_2 = \arctan[(y - y_{2,0})/(x - x_{2,0})]$, where the initial positions of the vortices (at $z = 0$) are given by the coordinates $(x_{1,0}, y_{1,0}) = (r_0, 0)$ and $(x_{2,0}, y_{2,0}) = (-r_0, 0)$ or, equivalently, $[R_1(0), \Theta_1(0)] = (r_0, 0)$ and $[R_2(0), \Theta_2(0)] = (r_0, \pi)$. The vortices are initially separated by a distance $d = 2r_0$.

Let us first examine the trajectories for a pair of r vortices, which, according to the theory reviewed in Section 3, are not expected to exhibit vortex–vortex (i.e., d -dependent) interactions. The trajectories demarcated on the intensity profile shown in Fig. 10 confirm this fact. The trajectory of the vortex at the initial point [in Cartesian coordinates $(r_0, 0)$] is exactly the same as that observed for the single r vortex shown in Fig. 8. In contrast, a pair of tanh vortices is expected to exhibit strikingly different propagation dynamics, depending on the separation distance d . Indeed, Fig. 11(a) shows that a significant rotation, 25° , is achieved over a short distance ($z/Z_0 = 0.1$). In comparison, the Gouy shift [Eq. (4)] over this distance is only 5.7° . As the vortex trajectory shows in Fig. 11(b), the rotation angles continue to increase over longer propagation distances; however, the radial positions also change. The vortices experience an initially rapid orbital motion, followed by a slower, nearly rectilinear motion. This trajectory is consistent with the discussion in Section 3, where it was argued that the singularities initially propagate like point vortices in a fluid

until the vortex cores begin to overlap. Experimental verification of this phenomenon were reported in Ref. 28.

Amplitude and phase gradients of the Gaussian beam also affect the trajectories, and thus we now investigate how the vortex dynamics is affected by both the beam size w_0 and the separation d . In Fig. 12 we have plotted numerically determined rotation angles as a function of distance for both linear and nonlinear propagation. (The nonlinear case is discussed in case 4 below.) In all three plots of Fig. 12 we find large initial rates of rotation [compared with the Gouy rate in Eq. (23)], as expected. However, we find a surprising result for the linear curve in Fig. 12(a), where we consider two closely spaced vortices in a large background field ($w_0 = 1464 \mu\text{m}$, $d/w_v = 2.40$, and $w_v = 57 \mu\text{m}$): The rotation angle, $\phi(z)$, indicates that the rotation reverses direction after some distance. This backward rotation may occur owing to two competing sources of amplitude gradients: the background Gaussian beam and the diffracting neighboring vortex. According to the vortex hypothesis, the effective background field that determines the motion of vortex 1 is given by the fields of both vortex 2 and the Gaussian beam. The gradient of the amplitude of the Gaussian beam is directed radially outward from the center of the beam, as usual; however, at some distance z it may be relatively weak compared with the amplitude gradient of the overlapping vortex. Thus the resultant direction of the amplitude gradient may switch directions as the diffracting envelope from one vortex begins to overlap the other; i.e., the background gradient may switch from being radially outward (with respect to the center of the beam) to radially inward. Therefore the direction of rotation, $m\mathbf{k} \times \nabla_{\perp} G_{\text{bg}}$ (where G_{bg} is the effective background field), may reverse.

Increasing the vortex separation distance may cause the vortices to rotate as quasi-point vortices for longer propagation distances, and thus larger rotation angles may be achieved. This result is verified in Fig. 12(b) for the case $d/w_v = 6.8$. In contrast, if the background

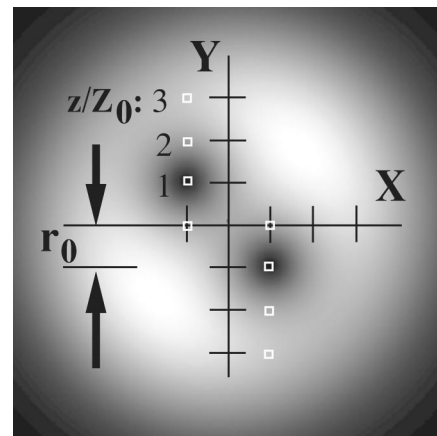


Fig. 10. Two r vortices of topological charge $m = +1$ and separation $d = 2r_0 = w_0 = 488 \mu\text{m}$ initially placed at points $(\pm r_0, 0)$. The beam, shown at a distance $z = Z_0$, shows the vortex rotation effect as described by the dynamic Gouy phase. The white open squares mark the positions of the vortices at propagation distances $z = 0, Z_0, 2Z_0, 3Z_0$. The trajectories are straight lines, as in Fig. 8.

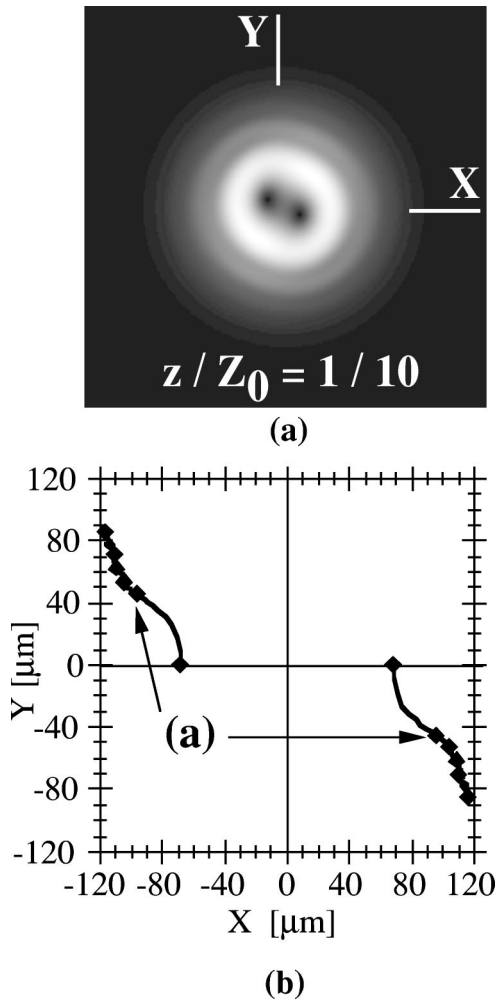


Fig. 11. (a) Two tanh vortices of topological charge $m = +1$ and separation $d = 2r_0 = 137 \mu\text{m}$ initially placed at points $(\pm r_0, 0)$ upon a Gaussian background beam of size $w_0 = 488 \mu\text{m}$. The beam, shown at a distance $z = 0.10 \times Z_0$, shows the vortex rotation effect. The projection of the vortex trajectories onto the transverse plane is depicted in (b), where filled diamonds mark propagation intervals of $\Delta z = Z_0/10$.

beam size, rather than d , is reduced, the amplitude gradient of the background beam may dominate the amplitude gradient of the neighboring vortex, resulting in no backward rotation effect. Indeed, this suggested effect is observed in Fig. 12(c) for the case $w_0 = 488 \mu\text{m}$, $d/w_v = 2.40$, and $w_v = 57 \mu\text{m}$. Note that Fig. 12 shows actual data points, not smoothed curves. The noise in the data for large values of z is a numerical artifact attributed to the uncertainty of the vortex position.

In each of the cases shown in Fig. 12 the initial rate of tanh vortex rotation exceeds that which occurs for r vortices [by 2 orders of magnitude in Fig. 12(a)]. However, our numerical data, shown in Fig. 13, suggest that this rate is not simply determined by the phase of the neighboring vortex, as expressed in Eq. (18), but also depends on the beam and vortex sizes, w_0 and w_v . (Note that the initial Gouy rates correspond to the values on the ordinate in Fig. 13.) We suggest corrections owing to amplitude gradients of both the background Gaussian beam and the neighboring tanh vortex, which we evaluate at a vortex core:

$$\begin{aligned} |\nabla_{\perp} A(r, z = 0)|_{r=d/2} & \\ &= 2A(r, z = 0) \\ &\quad \times (r/w_0^2 + 1/\{w_v \sinh[(r + d/2)/w_v]\})|_{r=d/2}. \end{aligned} \quad (24)$$

Applying the same method used to obtain Eq. (12), we determine a correction to Eq. (18), $\Omega'(z = 0)$, such that the initial rotation rate for tanh vortices can be written as

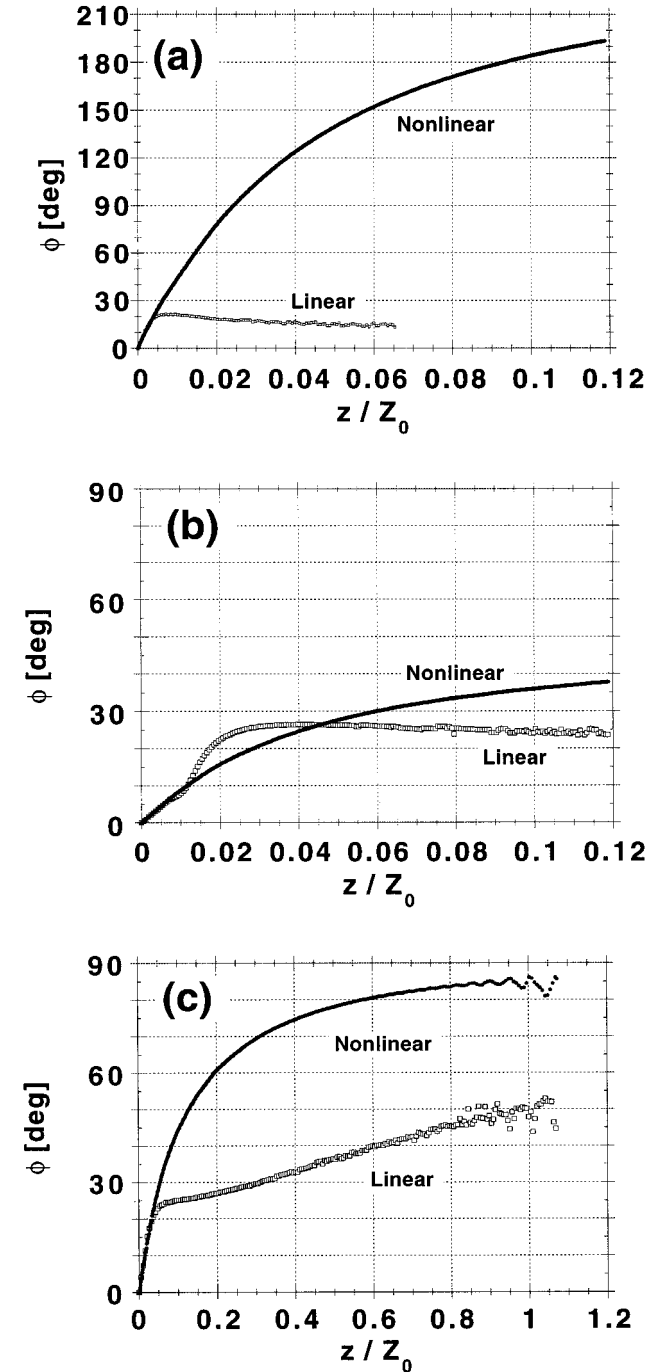


Fig. 12. Angle of rotation ϕ versus propagation distance z in linear and nonlinear media for a pair of tanh vortices of size $w_v = 57 \mu\text{m}$ and separation d upon a Gaussian background beam of size w_0 : (a) $d = 137 \mu\text{m}$, $w_0 = 1464 \mu\text{m}$ ($Z_0 = 8.4 \text{ m}$); (b) same as (a) except that $d = 390 \mu\text{m}$; (c) same as (a) except that $w_0 = 488 \mu\text{m}$ ($Z_0 = 0.94 \text{ m}$).

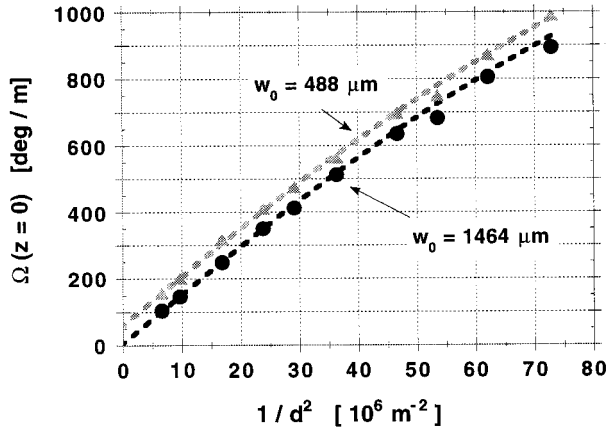


Fig. 13. Initial rate of tanh vortex pair rotation $\Omega(z=0)$ plotted for different separation distances d and background beam sizes w_0 . The dashed curves are theoretical curves from Eq. (25) with no adjustable parameters. Note that Fig. 12 indicates that $\Omega(z=0)$ is the same for both linear and nonlinear propagation.

$$\begin{aligned}\Omega_{\text{tanh}}(z=0) &= \Omega_d + \Omega'(z=0) \\ &= (\lambda/\pi)\{d^{-2} + w_0^{-2} \\ &\quad - 2/[dw_v \sinh(2d/w_v)]\}.\end{aligned}\quad (25)$$

The dashed curves in Fig. 13 show that the theoretical curves from Eq. (25) agree remarkably well with the numerical data (no adjustable parameters have been used).

D. Case 4

In self-defocusing nonlinear media, vortices may propagate as solitons, and hence the problems with diffracting tanh vortices (discussed in case 3) can be avoided, thereby permitting anomalously large vortex rotation angles. The core size of an OVS is approximately given by^{36,45}

$$w_v = 1.270k^{-1}(n_0/\Delta n_{\text{NL}})^{-1/2}, \quad (26)$$

where $\Delta n_{\text{NL}} = -n_2 E_0^2/2$ is a characteristic change of refractive index, n_2 is the coefficient of nonlinearity ($n_2 < 0$), and n_0 is the linear refractive index. For an OVS with $w_v = 57 \mu\text{m}$, the intensity of the beam must be adjusted to yield a nonlinear index change of $\Delta n = 1.6 \times 10^{-5}$ (assuming that $\lambda = 800 \text{ nm}$ and $n_0 = 1$). Although this value can be achieved in some materials, the propagation distances required for the rotations to be observed can be large (by optical material standards): of the order of $4\pi w_v^2/\lambda$, or at least 51 mm. Shorter optical path lengths require not only larger values of Δn but also a precise means of creating closely spaced vortices that have small cores. Fortunately, numerical simulations do not suffer from these restrictions, and we can investigate a variety of configurations to determine which may be most suitable for experiments.

Let us now examine the nonlinear propagation dynamics of OVS's, assuming the same initial field used in case 3 for tanh vortices. The resulting intensity profiles are shown in Fig. 14 for three different near-field propagation distances for the case $w_0 = 1464 \mu\text{m}$, $d/w_v = 2.40$, and $w_v = 57 \mu\text{m}$. The intensity profile after propagation of a distance $z/Z_0 = 0.01$ into the self-defocusing material is

depicted in Fig. 14(b), showing a rotation angle roughly 2 orders of magnitude larger than the Gouy phase at this distance. What is more, Figs. 14(c) and 14(d) demonstrate that rotation angles of 180° and greater are possible. This result significantly exceeds the 90° limit of the Gouy phase described by Eq. (4). Owing to self-defocusing and diffraction of the background beam, the vortices not only rotate but also move radially outward as the beam propagates. The resulting trajectory is a spiral shape, shown in Fig. 14(d).

We note that in Fig. 14(c) the amplitude profile of the background beam appears relatively uniform, which is characteristic of the optical blooming of a Gaussian laser beam in self-defocusing media. However, the intensity in the region near the vortices is nonuniform; hence, in a nonlinear medium, the phase will also be nonuniform. Let us assume that the vortex on the right-hand side of Fig. 14(c) resides in a nonuniform background field, G .

The amplitude gradient may contribute not only to a counterrotation in the $m\mathbf{k} \times \nabla_{\perp} G$ direction, as discussed in Section 3, but also a translation, owing to the nonlinear term in the phase: $m\theta + \Phi - kz[1 + (n_2/n_0)|G|^2]$, i.e., $\Phi_{\text{NL}} = -(n_2/n_0)|G|^2 kz$. Based on the fluid paradigm (see Section 3) the nonlinear contribution to the transverse momentum of the vortex should therefore be given by

$$\mathbf{k}_{\perp}^{(\text{NL})} = -\nabla_{\perp} \Phi_{\text{NL}} = +(kzn_2/n_0)\nabla_{\perp}|G|^2 \quad (27)$$

when evaluated at the vortex core. In self-defocusing media, $n_2 < 0$, and thus the right-hand vortex in Fig.

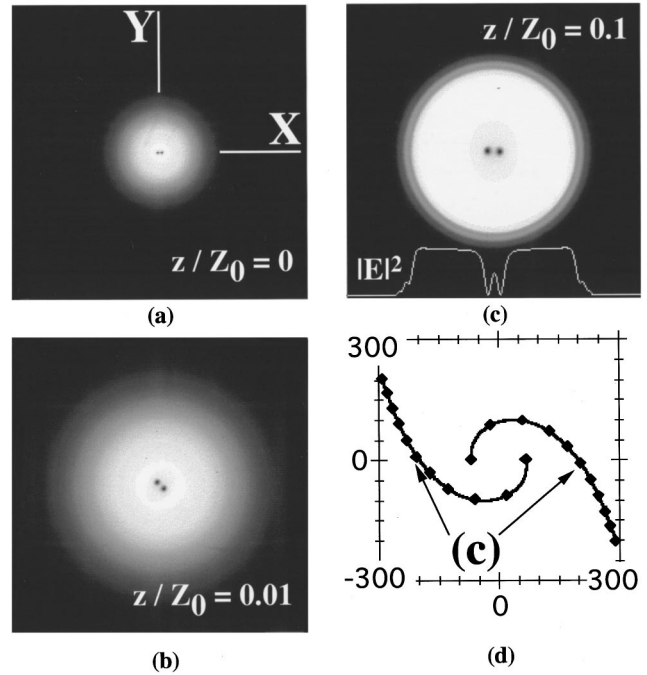


Fig. 14. Propagation of OVS's of charge $m = +1$, with initial conditions (a) $d = 137 \mu\text{m}$, $w_v = 57 \mu\text{m}$, $w_0 = 1464 \mu\text{m}$. A large clockwise rotation is evident over a short distance in (b), with a rotation angle greater than 180° demonstrated in (c). The projections of vortex trajectories onto the transverse plane are shown in (d), where filled diamonds mark propagation intervals of $\Delta z = Z_0/50$.

14(c) (which experiences a positive gradient owing to the vortex on the left) should be attracted to the neighboring vortex. Thus, in a nonlinear medium, vortices (of any sign or charge) experience attraction in addition to motions governed by the linear part of the system. Owing to the rotational motion of the vortices and to the nonlinear attraction, stable orbits may be possible. Preliminary numerical investigations confirm such orbital motion.

Although nonlinear effects complicate the description of OVS rotation, we propose that an experiment could achieve results similar to the numerical results shown in Fig. 12(a), achieving rotation angles in excess of the Gouy limit of 90° (see the curve labeled Nonlinear). It is also possible to observe the opposite effect, namely, less rotation in the nonlinear case than in the linear case, as numerical calculations indicate in Fig. 12(b). This somewhat anomalous effect may already have been observed⁵⁷; however, in that case OVS's were probably not achieved, owing to the use of a short-focal-length lens in front of the nonlinear cell. Another experimentally observable effect occurs when the beam size is made small. In this case our numerical results, shown in Fig. 12(c), indicate that it is possible to enhance the rotation angle (by a factor of 2 in this case) in a nonlinear medium but still not exceed 90° in the near-field region.

5. CONCLUSIONS

We have examined three factors that affect the motion of optical vortices: an amplitude gradient, a phase gradient, and a nonlinear factor that depends on the intensity gradient, and found that these factors qualitatively and quantitatively describe the trajectories observed in our numerical investigations. We found contrasting differences between the trajectories for r vortices that have globally distributed core functions and tanh vortices that have localized core functions when the beam propagates through a linear medium. In particular, identical localized vortices with nonoverlapping cores were found to orbit each other at a rate that depends inversely on the squared vortex separation distance. This latter phenomenon is analogous to the rotation of point vortices in fluid dynamics. In a linear medium vortices diffract, becoming nonlocalized; hence the maximum rotation angle of the vortex pair is limited. However, in a self-defocusing medium the vortices may propagate as nondiffracting optical vortex solitons, and thus anomalously large rotation angles may be achieved. What is more, stable orbits may be possible, owing to an attractive nonlinear interaction between the rotating solitons.

ACKNOWLEDGMENTS

G. A. Swartzlander was supported by the Research Corporation as a Cottrell Scholar and by the National Science Foundation as a Young Investigator. C. T. Law was supported by the National Science Foundation CAREER program.

REFERENCES

1. J. F. Nye and M. V. Berry, "Dislocations in wave trains," *Proc. R. Soc. London Ser. A* **336**, 165–190 (1974).
2. M. V. Berry, "Singularities in waves and rays," in *Physics of Defects*, R. Balian, M. Kleman, and J.-P. Poirier, eds. (North-Holland, Amsterdam, 1981), pp. 453–543.
3. N. B. Baranova, B. Ya. Zel'dovich, A. V. Mamaev, N. F. Pilipetskii, and V. V. Shkukov, "Dislocations of the wavefront of a speckle-inhomogeneous field (theory and experiment)," *Pis'ma Zh. Eksp. Teor. Fiz.* **33**, 206–210 (1981) [*JETP Lett.* **33**, 195–199 (1981)].
4. N. B. Baranova, A. V. Mamaev, N. F. Pilipetskii, V. V. Shkukov, and B. Ya. Zel'dovich, "Wavefront dislocations: topological limitations for adaptive systems with phase conjugation," *J. Opt. Soc. Am.* **73**, 525–528 (1983).
5. G. Goubau and F. Schwering, "On the guided propagation of electromagnetic wave beams," *IRE Trans. Antennas Propag.* **9**, 248–256 (1961).
6. J. M. Vaughan and D. V. Willetts, "Temporal and interference fringe analysis of TEM₀₁* laser modes," *J. Opt. Soc. Am.* **73**, 1018–1021 (1983).
7. A. G. White, C. P. Smith, N. R. Heckenberg, H. Rubinsztein-Dunlop, R. McDuff, C. O. Weiss, and Chr. Tamm, "Interferometric measurements of phase singularities in the output of a visible laser," *J. Mod. Opt.* **38**, 2531–2541 (1991).
8. E. Abramochkin and V. Volostnikov, "Beam transformations and nontransformed beams," *Opt. Commun.* **83**, 123–135 (1991).
9. L. M. Pismen and A. A. Nepomnyashchy, "On interaction of spiral waves," *Physica D* **54**, 183–193 (1992).
10. V. Yu. Bazhenov, M. S. Soskin, and M. V. Vasnetsov, "Screw dislocations in light wavefronts," *J. Mod. Opt.* **39**, 985–990 (1992).
11. S. N. Khonina, V. V. Kotlyar, M. V. Shinkaryev, V. A. Soifer, and G. V. Uspleniev, "The phase rotor filter," *J. Mod. Opt.* **39**, 1147–1154 (1992).
12. N. R. Heckenberg, R. McDuff, C. P. Smith, H. Rubinsztein-Dunlop, and M. J. Wegener, "Laser beams with phase singularities," *Opt. Quantum Electron.* **24**, S951–S962 (1992).
13. I. V. Basistiy, V. Yu. Bazhenov, M. S. Soskin, and M. V. Vasnetsov, "Optics of light beams with screw dislocations," *Opt. Commun.* **103**, 422–428 (1993).
14. G. Indebetouw, "Optical vortices and their propagation," *J. Mod. Opt.* **40**, 73–87 (1993).
15. M. W. Beijersbergen, R. P. C. Coerwinkel, M. Kristensen, and J. P. Woerdman, "Helical-wavefront laser beams produced with a spiral phaseplate," *Opt. Commun.* **112**, 321–327 (1994).
16. F. B. de Colstoun, G. Khitrova, A. V. Fedorov, T. R. Nelson, C. Lowry, T. M. Brennan, B. G. Hammons, and P. D. Maker, "Transverse modes, vortices and vertical-cavity surface-emitting lasers," *Chaos Solitons Fractals* **4**, 1575–1596 (1994).
17. F. S. Roux, "Dynamical behavior of optical vortices," *J. Opt. Soc. Am. B* **12**, 1215–1221 (1995).
18. P. Couillet, L. Gil, and F. Rocca, "Optical vortices," *Opt. Commun.* **73**, 403–408 (1989).
19. G. L. Lippi, T. Ackemann, L. M. Hoffer, A. Gahl, and W. Lange, "Interplay of linear and nonlinear effects in the formation of optical vortices in a nonlinear resonator," *Phys. Rev. A* **48**, R4043–R4046 (1993).
20. M. Brambilla, M. Cattaneo, L. A. Lugiato, R. Pirovano, F. Pratti, A. J. Kent, G.-L. Oppo, A. B. Coates, C. O. Weiss, C. Green, E. J. D'Angelo, and J. R. Tredicce, "Dynamical transverse laser patterns. I. Theory," *Phys. Rev. A* **49**, 1427–1451 (1994).
21. G. Indebetouw and D. R. Korwan, "Model of vortices nucleation in a photorefractive phase-conjugate resonator," *J. Mod. Opt.* **41**, 941–950 (1994).
22. G. Slekyas, K. Staliunas, and C. O. Weiss, "Motion of phase singularities in a class-B laser," *Opt. Commun.* **119**, 433–446 (1995).
23. K. Staliunas and C. O. Weiss, "Nonstationary vortex lat-

- tices in large-aperture class B lasers," *J. Opt. Soc. Am. B* **12**, 1142–1149 (1995).
24. N. R. Heckenberg, M. Vaupel, J. T. Malos, and C. O. Weiss, "Optical-vortex pair creation and annihilation and helical astigmatism of a nonplanar ring resonator," *Phys. Rev. A* **54**, 1–10 (1996).
 25. W. J. Firth and A. Lord, "Two-dimensional solitons in a Kerr cavity," *J. Mod. Opt.* **43**, 1071–1077 (1996).
 26. V. Yu. Bazhenov, M. V. Vasnetsov, and M. S. Soskin, "Laser beams with screw dislocations in their wavefronts," *Pis'ma Zh. Eksp. Teor. Fiz.* **52**, 1037–1039 (1990) [*JETP Lett.* **52**, 429–431 (1990)].
 27. N. R. Heckenberg, R. McDuff, C. P. Smith, and A. G. White, "Generation of optical phase singularities by computer-generated holograms," *Opt. Lett.* **17**, 221–223 (1992).
 28. G. A. Swartzlander, Jr., Z. Sacks, X. Zhang, D. Rozas, and C. T. Law, "Formation and propagation of optical vortices," in *Digest of the International Quantum Electronics Conference*, 1996 OSA Technical Digest Series (Optical Society of America, Washington, D.C., 1996), p. 31; D. Rozas, Z. S. Sacks, and G. A. Swartzlander, Jr., "Experimental observations of fluid-like motion of optical vortices," *Phys. Rev. Lett.* (to be published).
 29. K. Staliunas, "Dynamics of optical vortices in a laser beam," *Opt. Commun.* **90**, 123–127 (1992).
 30. K. Staliunas, "Optical vortices during three-way nonlinear coupling," *Opt. Commun.* **91**, 82–86 (1992).
 31. I. Freund, N. Shvartsman, and V. Freilikher, "Optical dislocation networks in highly random media," *Opt. Commun.* **101**, 247–264 (1993).
 32. I. Freund, "Optical vortices in Gaussian random wave fields: statistical probability densities," *J. Opt. Soc. Am. A* **11**, 1644–1652 (1994).
 33. K. Staliunas, A. Berzanskis, and V. Jarutis, "Vortex statistics in optical speckle fields," *Opt. Commun.* **120**, 23–28 (1995).
 34. C. O. Weiss, H. R. Telle, and K. Staliunas, "Restless optical vortex," *Phys. Rev. A* **47**, R1616–R1619 (1993).
 35. D. Y. Tang, N. R. Heckenberg, and C. O. Weiss, "Phase-dependent helical pattern formation in a laser," *Opt. Commun.* **114**, 95–100 (1995).
 36. G. A. Swartzlander, Jr., and C. T. Law, "Optical vortex solitons observed in Kerr nonlinear media," *Phys. Rev. Lett.* **69**, 2503–2506 (1992).
 37. G. A. Swartzlander, Jr., and C. T. Law, "The optical vortex soliton," *Opt. Photonics News* **4**(12), 10 (1993).
 38. A. V. Mamaev, M. Saffman, D. Z. Anderson, and A. A. Zozulya, "Propagation of light beams in anisotropic nonlinear media: from symmetry breaking to spatial turbulence," *Phys. Rev. A* **54**, 870–879 (1996).
 39. A. V. Mamaev, M. Saffman, and A. A. Zozulya, "Break-up of two-dimensional bright spatial solitons due to transverse modulation instability," *Europhys. Lett.* **35**, 25–30 (1996).
 40. A. V. Mamaev, M. Saffman, and A. A. Zozulya, "Propagation of dark stripe beams in nonlinear media: snake instability and creation of optical vortices," *Phys. Rev. Lett.* **76**, 2262–2265 (1996).
 41. V. Tikhonenko, J. Christou, B. Luther-Davies, and Yu. S. Kivshar, "Observation of vortex solitons created by the instability of dark soliton stripes," *Opt. Lett.* **21**, 1129–1131 (1996).
 42. G. S. McDonald, K. S. Syed, and W. J. Firth, "Optical vortices in beam propagation through a self-defocusing medium," *Opt. Commun.* **94**, 469–476 (1992).
 43. A. W. Snyder, L. Poladian, and D. J. Mitchell, "Stable black self-guided beams of circular symmetry in a bulk Kerr medium," *Opt. Lett.* **17**, 789–791 (1992).
 44. R. Y. Chiao, I. H. Deutsch, J. C. Garrison, and E. M. Wright, in *Serge Akhmanov: A Memorial Volume*, H. Walther, ed. (Hilger, Bristol, UK, 1992), pp. 151–182.
 45. C. T. Law and G. A. Swartzlander, Jr., "Optical vortex solitons and the stability of dark soliton stripes," *Opt. Lett.* **18**, 586–588 (1993).
 46. G. S. McDonald, K. S. Syed, and W. J. Firth, "Dark spatial soliton break-up in the transverse plane," *Opt. Commun.* **95**, 281–288 (1993).
 47. K. Staliunas, "Vortices and dark solitons in the two-dimensional nonlinear Schrödinger equation," *Chaos Solitons Fractals* **4**, 1783–1796 (1994).
 48. C. T. Law and G. A. Swartzlander, Jr., "Polarized optical vortex solitons: instabilities and dynamics in Kerr nonlinear media," *Chaos Solitons Fractals* **4**, 1759–1766 (1994).
 49. I. Velchev, A. Dreischuh, D. Neshev, and S. Dinev, "Interactions of optical vortex solitons superimposed on different background beams," *Opt. Commun.* **130**, 385–392 (1996).
 50. Y. Chen and J. Atai, "Dynamics of optical-vortex solitons in a perturbed nonlinear medium," *J. Opt. Soc. Am. B* **11**, 2000–2003 (1994).
 51. J. Christou, V. Tikhonenko, Yu. S. Kivshar, and B. Luther-Davies, "Vortex soliton motion and steering," *Opt. Lett.* **21**, 1649–1651 (1996).
 52. See, for example, M. S. El Naschie, ed., "Special issue on nonlinear optical structures, patterns, chaos," *Chaos Solitons Fractals* **4**(8/9) (1994).
 53. E. M. Wright, R. Y. Chiao, and J. C. Garrison, "Optical anyons: atoms trapped on electromagnetic vortices," *Chaos Solitons Fractals* **4**, 1797–1803 (1994).
 54. G. Duree, M. Morin, G. Salamo, M. Segev, B. Crosignani, P. DiPorto, E. Sharp, and A. Yariv, "Dark photorefractive spatial solitons and photorefractive vortex solitons," *Phys. Rev. Lett.* **74**, 1978–1981 (1995).
 55. M. Morin, G. Duree, and M. Segev, "Waveguides formed by quasi-steady-state photorefractive spatial solitons," *Opt. Lett.* **20**, 2066–2068 (1995).
 56. J. Feinberg, "Asymmetric self-defocusing of an optical beam from the photorefractive effect," *J. Opt. Soc. Am.* **72**, 46–51 (1982).
 57. B. Luther-Davies, R. Powles, and V. Tikhonenko, "Nonlinear rotation of three-dimensional dark spatial solitons in a Gaussian laser beam," *Opt. Lett.* **19**, 1816–1818 (1994).
 58. T. Ackemann, E. Kriege, and W. Lange, "Phase singularities via nonlinear beam propagation in sodium vapor," *Opt. Commun.* **115**, 339–346 (1995).
 59. V. L. Ginzburg and L. P. Pitaevskii, "On the theory of superfluidity," *Zh. Eksp. Teor. Fiz.* **34**, 1240–1245 (1958) [*Sov. Phys. JETP* **7**, 858–861 (1958)].
 60. L. P. Pitaevskii, "Vortex lines in an imperfect Bose gas," *Zh. Eksp. Teor. Fiz.* **40**, 646–651 (1961) [*Sov. Phys. JETP* **13**, 451–454 (1961)].
 61. P. G. de Gennes, *Superconductivity of Metals and Alloys* (Addison-Wesley, Reading, Mass., 1989); R. J. Donnelly, *Quantized Vortices in Helium II* (Cambridge U. Press, New York, 1991).
 62. A. L. Fetter, "Vortices in an imperfect Bose gas," *Phys. Rev.* **138**, A429–A431 (1965).
 63. G. A. Askar'yan, "Effects of the gradient of a strong electromagnetic beam on electrons and atoms," *Sov. Phys. JETP* **15**, 1088–1090 (1962).
 64. A. Ashkin, "Forces of a single-beam gradient laser trap on a dielectric sphere in array optic regime," *Biophys. J.* **61**, 569–582 (1992).
 65. M. W. Beijersbergen, L. Allen, H. E. L. O. van der Veen, and J. P. Woerdman, "Astigmatic laser mode converters and transfer of orbital angular momentum," *Opt. Commun.* **96**, 123–132 (1993).
 66. H. He, M. E. J. Friese, N. R. Heckenberg, and H. Rubinsztein-Dunlop, "Direct observation of transfer of angular momentum to absorptive particles from a laser beam with a phase singularity," *Phys. Rev. Lett.* **75**, 826–829 (1995).
 67. H. He, N. R. Heckenberg, and H. Rubinsztein-Dunlop, "Optical particle trapping with higher-order doughnut beams produced using high-efficiency computer generated holograms," *J. Mod. Opt.* **42**, 217–223 (1995).
 68. K. T. Gahagan and G. A. Swartzlander, Jr., "Optical vortex trapping of particles," *Opt. Lett.* **21**, 827–829 (1996).
 69. A. E. Siegman, *Lasers* (University Science Books, Mill Valley, Calif., 1986).
 70. L. G. Gouy, "Sur la propagation anormale des ondes," *Ann. Chim. Phys. Ser. 6* **24**, 145–213 (1891).
 71. J. H. Goodman, *Introduction to Fourier Optics* (McGraw-Hill, New York, 1968).

72. W. G. Wagner, H. A. Haus, and J. H. Marburger, "Large-scale self-trapping of optical beams in the paraxial ray approximation," *Phys. Rev.* **175**, 256–266 (1968).
73. C. Nore, M. E. Brachet, and S. Fauve, "Numerical study of hydrodynamics using the nonlinear Schrödinger (NLS) equation," *Physica D* **65**, 154–162 (1993).
74. L. M. Milne-Thomson, *Theoretical Hydrodynamics* (Macmillan, New York, 1968).
75. M. D. Feit and J. A. Fleck, Jr., "Light propagation in graded-index optical fibers," *Appl. Opt.* **17**, 3990–3998 (1978).